JGR Space Physics

RESEARCH ARTICLE
10.1029/2020JA028003

On the Seeding of Periodic Equatorial Plasma Bubbles by Gravity Waves Associated With Tropical Cyclone: A Case Study

K. K. Ajith[1], Guozhu Li[1,2,3], S. Tulasi Ram[4], M. Yamamoto[5], K. Hozumi[6], Prayitno Abadi[7], and Haiyong Xie[1,2]

[1]Key Laboratory of Earth and Planetary Physics, Institute of Geology and Geophysics, Chinese Academy of Sciences, Beijing, China, [2]Beijing National Observatory of Space Environment, Institute of Geology and Geophysics, Chinese Academy of Sciences, Beijing, China, [3]College of Earth and Planetary Sciences, University of Chinese Academy of Sciences, Beijing, China, [4]Indian Institute of Geomagnetism, Mumbai, India, [5]Research Institute for Sustainable Humanosphere, Kyoto University, Uji, Japan, [6]National Institute of Information and Communications Technology, Tokyo, Japan, [7]Space Science Center, Indonesian National Institute of Aeronautics and Space (LAPAN), Bandung, Indonesia

Key Points:

- GW seeding of periodic and intense presunset EPBs was observed on 8 and 9 April 2013 in connection with the deep convection associated with tropical cyclone Victoria
- The GPS-TEC observation shows clear GW signatures with ~300-km wavelength, ~23-min periodicity, and horizontal velocity of ~225 m/s
- The observed GW parameters indicate the possibility of EPB seeding due to the secondary GWs generated by the dissipation of primary GWs at the middle atmosphere

Correspondence to:
K. K. Ajith and G. Li,
ajithkk2007@gmail.com;
gzlee@mail.iggcas.ac.cn

Citation:
Ajith, K. K., Li, G., Tulasi Ram, S., Yamamoto, M., Hozumi, K., Abadi, P., & Xie, H. (2020). On the seeding of periodic equatorial plasma bubbles by gravity waves associated with tropical cyclone: A case study. *Journal of Geophysical Research: Space Physics*, *125*, e2020JA028003. https://doi.org/10.1029/2020JA028003

Received 11 MAR 2020
Accepted 26 SEP 2020
Accepted article online 5 OCT 2020

Abstract Understanding the day-to-day variability of equatorial plasma bubble (EPB) irregularities has been a major challenge for many decades that makes the deterministic prediction of EPBs remain elusive. In the present study, we report a case of intense and periodic EPBs observed during 8 and 9 April 2013 by the 47-MHz Equatorial Atmosphere Radar at Kototabang, Indonesia. The periodic EPBs separated by about 200–250 km were initiated before sunset. The presunset onset and development of these periodic EPBs were discussed in light of the gravity waves (GWs) excited in connection with the deep convection due to the tropical cyclone (TC) Victoria. The outgoing long-wave radiation measurement by very high-resolution radiometer (VHRR) onboard Indian meteorological satellite Kalpana-1 shows the occurrence of deep convective activity during these days. The presence of upward propagating GWs from the deep convective region associated with TC Victoria was confirmed using the GPS radio occultation (GPS-RO) observations in the troposphere and stratosphere. The GW signatures at ionospheric altitudes were also observed from the Ionosonde observations over magnetic equator, and medium-scale (~300 km) GWs were observed from the GPS-TEC (Total Electron Content) data near to the magnetic equator and cyclone center. From the GW parameters observed from GPS-TEC and GPS-RO, we surmise that the secondary GWs generated by the dissipation of primary GWs associated with TC Victoria could have served as a seeding source on the generation of periodic EPBs during these two consecutive days.

1. Introduction

Equatorial plasma bubbles (EPBs) are the plasma density-depleted regions in the nighttime equatorial *F* region. These plasma density irregularities manifest as diffused echoes in the ionograms, backscatter plumes in very high frequency (VHF) radar maps, intensity bite outs in night time OI 630-nm airglow emissions, density depletions in the in situ satellite measurements, and scintillations in VHF/L-band satellite beacon signals (Aarons, 1982; Abdu et al., 1982; Ajith et al., 2015; Otsuka et al., 2002; Rama Rao et al., 2005; Watthanasangmechai et al., 2016; Woodman & LaHoz, 1976). Since these plasma irregularities can cause severe outages in the satellite-based communication and navigation systems, understanding the day-to-day variability of this phenomenon is one of the important topics of space weather interest. According to our present understanding, the Rayleigh-Taylor (RT) instability at the bottom side F region is believed as the fundamental process responsible for the development of EPBs (Haerendel, 1973). The rapid uplift of *F* layer due to the Pre-reversal Enhancement (PRE) of zonal electric field and steep vertical density gradient at the bottom side *F* region by the quick recombination of plasma makes the conditions favorable for the development of EPBs just after the sunset (Farley et al., 1986; Fejer et al., 1991).

From the extensive studies during past several decades, the seasonal, local time, and solar activity effect on the EPB occurrence were grossly understood (Abdu et al., 1981; Li et al., 2007, 2013; Tulasi Ram et al., 2006). The studies on the solar activity dependence of the EPB occurrence show that the occurrence probability is more prominent during high solar active periods (Basu et al., 1988). Further, it is generally understood that

the EPB occurrence is largest for the equatorial locations where, and the seasons when, the local magnetic field lines align with the sunset terminator (Abdu et al., 1981; Tsunoda, 1985). More specifically, in the Southeast Asian longitude sector, the declination angle of the geomagnetic field line is nearly zero, and the EPB occurrence is generally higher during the equinoxes compared to solstice months. However, observational studies often vindicate the suppression of EPB development in some nights even during equinox and enhancement during some solstice nights (Ajith et al., 2018; Carter et al., 2018). This unusual suppression/development of EPBs leads enigmatic day-to-day variability on the occurrence of EPBs even under quiet geomagnetic conditions. It concludes that the PRE and postsunset height rise (PSSR) are necessary but not sufficient criteria for the onset of EPBs. This has led to the investigation on the plausible role of seeding source for the RT instability, which would explain the day-to-day variability observed in the EPB occurrence. It has been reported that the upward propagating gravity waves (GWs) are one of the major sources for the required initial seed perturbations for the development of EPBs (Hysell et al., 1990; Kelley et al., 1981; Singh et al., 1997). There are several observational evidences for this GW seeding of EPBs by different observational techniques such as VHF radars, satellite in situ, LIDAR, Mesosphere Stratosphere Troposphere (MST) radar, Airglow imager, and Ionosonde (e.g., Abdu et al., 2009; Kelley et al., 1986; Nicolls & Kelley, 2005; Sivakandan et al., 2019; Takahashi et al., 2009; Taori et al., 2011; Tsunoda & White, 1981). Additionally, several numerical modeling studies also support the GW seeding of EPBs (Huang & Kelley, 1996; Klostermeyer, 1978; Krall et al., 2013; Yokoyama et al., 2019). The GWs, which generated at lower atmospheric altitudes with sufficient energy and vertical wavelength, can reach ionospheric heights directly without dissipation (Vadas, 2007) or the primary GWs may break into secondary waves at mesospheric altitudes and these secondary waves can propagate to the ionospheric altitudes (Fritts & Alexander, 2003; Hung & Smith, 1978; Vadas & Crowley, 2010; Vadas & Fritts, 2006).

There are several studies, which reported the presence of large-scale wave like structure (LSWS) before the onset of EPBs (Kelley et al., 1981; Rottger, 1973; Tsunoda & White, 1981). Further, it is believed that the EPBs in general start to develop from the crests of this spatial wave like structure and may lead this to the development of periodic EPBs (Thampi et al., 2009; Tsunoda, 2015; Tulasi Ram et al., 2012). Makela et al. (2010) presented the distribution of spacing between EPBs observed using an airglow imaging system located in Chile. They have observed periodic spacing between EPBs during 123 nights out of 317 days of observations and argued that the GW seeding as the underlying factor for the development of these periodic EPBs. Using C/NOFS satellite observations, Huang et al. (2013) reported the periodic development of EPBs, and they have proposed a mechanism based on the GW seeding in the postsunset sector. However, the studies of Huang et al. (2013) and Makela et al. (2010) focused only on the periodic EPBs and not showing any simultaneous GW observations. Hence, it is important to study the periodic EPB structures along with simultaneous GW measurements and background ionospheric conditions to obtain a deep insight on the seeding mechanism of EPBs.

One of the major sources of GW is the tropospheric convective regions from where these waves propagate upward at slant angles with increasing amplitudes to ionospheric heights (Fritts & Alexander, 2003; Fritts & Nastrom, 1992). Hence, in order to see the possible relationship between GW seeding and EPB development, several studies have been carried out on the correlation between convective activity in the lower atmosphere and EPB occurrence (McClure et al., 1998; Rottger, 1981; Tsunoda, 2010). Using the Outgoing Long-wave Radiation (OLR) map and ESF climatology data, Tsunoda (2010) has shown that the ESF occurrence is controlled by the seasonal migration of Intertropical Convergence Zone (ITCZ), especially during solstice. Further, the results obtained from the SpreadFEx campaign show the relationship between mesospheric GWs linked with deep convection to the plasma bubble seeding in the ionosphere (Abdu et al., 2009; Fritts et al., 2009; Takahashi et al., 2009). Recently, Li et al. (2016) examined the development of fresh EPBs over Kototabang and Sanya using two VHF radars. They have observed an enhanced development of fresh EPBs over Kototabang as compared to Sanya and attributed this to the higher GW activity associated with ITCZ over Kototabang.

Among the convective GW sources, the GWs associated with the tropical cyclones (TCs) and its effects on ionospheric plasma have called special attention for investigation. Using ionosonde data, for the first time, Bauer (1958) reported an increase in fo*F*2 followed by the nearby passage of a hurricane. Later, several studies reported the effect of TCs on ionospheric plasma such as effect on *F* region plasma drift and development of medium-scale traveling ionospheric disturbances (MSTIDs) (Bishop et al., 2006; Hung &

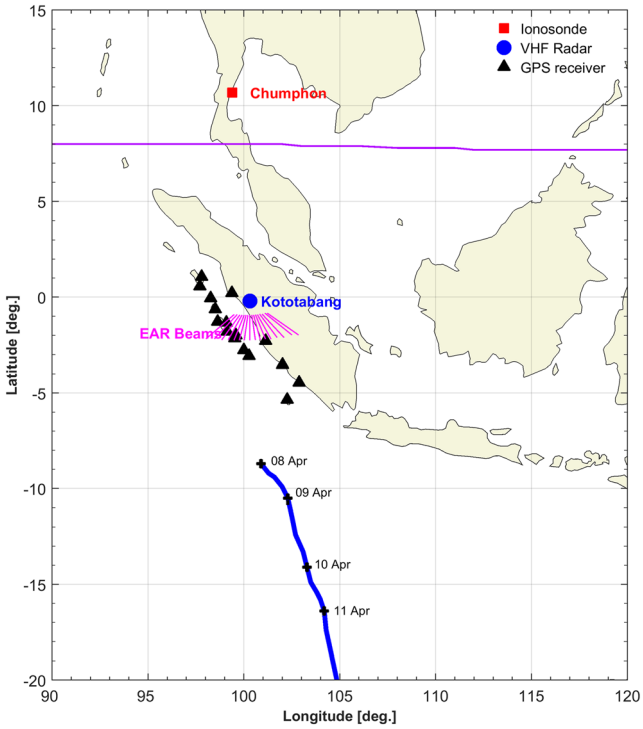

Figure 1. The geographic locations of the VHF radar, Ionosonde, and GPS receivers used in the present study. The thick blue curve indicates the trajectory of TC Victoria.

Table 1
List of GPS Stations Used in This Study

Station code	Latitude	Longitude
ABGS	00.22°N	99.39°E
BITI	01.08°N	97.81°E
BSAT	03.07°S	100.28°E
BTET	01.28°S	98.64°E
BTHL	00.57°N	97.71°E
LAIS	03.52°S	102.03°E
LNNG	02.28°S	101.15°E
MLKN	05.35°S	102.27°E
MNNA	04.45°S	102.89°E
MSAI	01.32°S	99.09°E
PBJO	00.63°S	98.52°E
PKRT	02.15°S	99.54°E
PPNJ	01.99°S	99.60°E
PTLO	00.05°S	98.28°E
SLBU	02.76°S	100.00°E
TLLU	01.80°S	99.13°E

Kao, 1978; Song et al., 2017; Xiao et al., 2007). The majority of MSTIDs observed at low-latitude ionosphere are manifestation of the upward propagating GWs due to meteorological processes (Buonsanto, 1999; Ding et al., 2011; Hines, 1960). Nishioka et al. (2013) have given a clear observational evidence of concentric waves developed in the ionosphere after the 2013 Moore EF5 tornado. Using the dense GPS network data from China, Song et al. (2019) reported the observation of two MSTID events during the Typhoon Chan-hom. Even though there are several studies that reported the development of MSTIDs and TIDs due to TCs, studies on the EPB/ESF irregularities associated with TCs are very few (Ke et al., 2019; Lou et al., 2019; Yang & Liu, 2016). These studies, which carried out mainly using GPS-TEC and scintillation measurements, could report the occurrence of EPBs associated with TCs; however, they were lack of the simultaneous observation of the responsible initial seed perturbations (GWs). The spatiotemporal evolution and drift characteristics of EPBs are hard to understand using GPS-TEC technique. In this study, we present a comprehensive investigation of the development of periodic EPBs and the simultaneous observation of the GWs associated with a TC named TC Victoria using multi-instrumental observations include GPS radio occultation (GPS-RO), Ionosonde, GPS-TEC, and Equatorial Atmosphere Radar (EAR) over Indonesian longitudes.

2. Data

The geographic locations of Chumphon ionosonde, GPS receivers from Sumatra GPS network, and beam directions of EAR are shown in Figure 1. The 47-MHz EAR at Kototabang, Indonesia (0.2°S geog. lat, 100.3°E geog. long, and 10.1°S dip. lat) is a coherent backscatter VHF radar operated with a peak and average power of 100 and 5 kW, respectively. Using the active phase arrayed 16-beam antenna system, EAR can steer on a pulse-to-pulse basis and detect the spatial and temporal evolution of ~3-m scale irregularities in the ionosphere (Fukao et al., 2003). In the present study, the backscatter fan sector maps and Altitude-Time-Intensity (ATI) maps obtained from EAR are used to examine the spatial and temporal variation of EPBs. We have used the GPS data from 16 stations of the GPS receiver network in Sumatra, Indonesia (Sumatran GPS Array (SuGAr)), which are close to EAR and dip equator. These stations are listed in Table 1 and represented as black triangles in Figure 1. The vertical TEC (VTEC) is computed from the GPS data using the GPS-TEC analysis application software developed at Boston College (Seemala, 2011).

According to Australian government Bureau of Meteorology, TC Victoria was developed as a low-pressure system in the Indian Ocean on 6 April 2013 and moved to the southeast direction and developed into a category 3 TC. The thick blue curve in Figure 1 shows the track of TC Victoria. The deep convective activity due to TC Victoria has been examined using the OLR observations from the very high-resolution radiometer (VHRR) on board the Indian meteorological geostationary satellite Kalpana-1 (Singh et al., 2007) and 4-km resolution IR brightness temperature data obtained from the Goddard Earth Sciences Data and Information Services Center (GES DISC) (Janowiak et al., 2017) over Indian and Indonesian region. The upward propagating GWs from the deep convective region near to TC Victoria have been analyzed using the GPS-RO temperature profiles obtained from COSMIC, MetOp-A, and MetOp-B satellites during 8 and

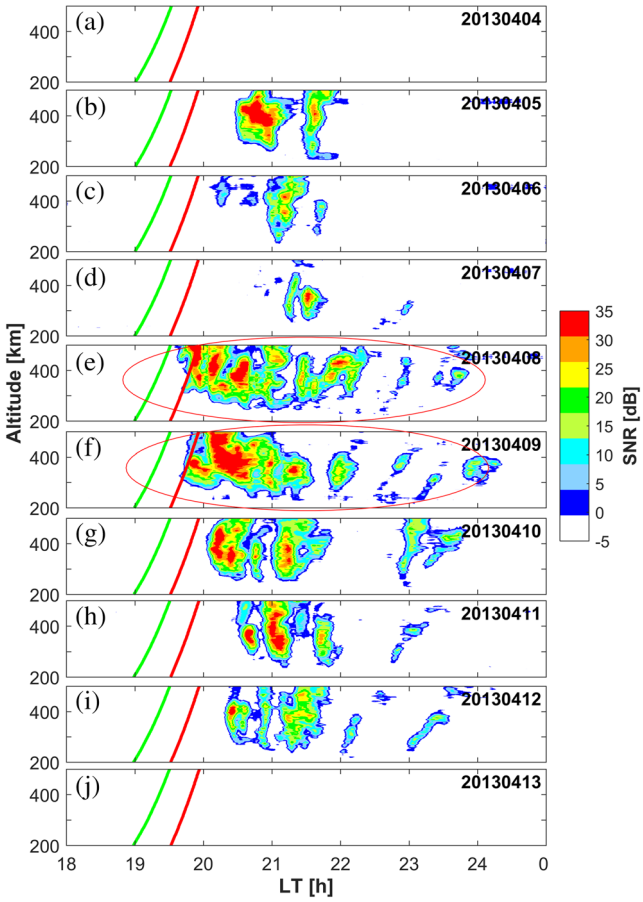

Figure 2. Altitude-time-intensity (ATI) maps of backscatter echo observed by the central beam (180°) of EAR during 4–13 April 2013. The green and red curves indicate the local and apex sunset.

9 April 2013. The "atmprf" data with 20-m vertical resolution were used to derive the temperature perturbations. The 5-min interval data obtained from the ionosonde operated at Chumphon (CPN) (10.7°N geog. lat., 99.4°E geog. long, and 3.3°N dip lat.) have been used to extract the GW signatures in the bottom side *F* layer heights (h'F) at specific plasma frequencies. The downward phase propagation of GWs can be detected using the *F* layer virtual height measurements at different frequencies (isofrequency lines) (Abdu et al., 2009, 2015; Takahashi et al., 2009). These isofrequency lines can be used to derive the GW parameters such as vertical phase velocity (V_z), period (T), and vertical wavelength (λ_z). A band pass filter with period between 20 and 90 min was used to extract the short-period oscillations in the h'F (Abdu et al., 2015).

3. Results

With a view to understand the GW seeding of EPBs associated with the deep convective activity over Indonesian longitudes due to TC Victoria, we examined the onset and development characteristics of EPBs observed from EAR during 10 consecutive days from 4 to 13 April 2013. During this month, the solar activity was moderately high with a monthly mean f10.7 of 129 solar flux units. Figure 2 shows the ATI plots of 3-m scale irregularities obtained from the central beam (180° azimuth) of EAR observed during 4–13 April 2013 over Kototabang, Indonesia. The green and red curves in Figure 2 indicate the local and apex sunset terminators at EAR longitude (100.32°E). As mentioned earlier in the text, a low-pressure region is developed on 6 April 2013 over south Indian ocean around 6°S, 99°E; however, it get intensified as a TC only on 8 April 2013 around 9.2°S, 101.6°E. From Figure 2, one can observe that during 4–07 April (before the onset of TC), EPBs were either absent or developed 30–60 min after the apex sunset, whereas on 8 and 9 April, the presence of continuous and intense EPBs with periodic structure has been observed during the premidnight hours. During these 2 days, the TC was already developed, and its center was closer to the geomagnetic equator as compared to other days. Interestingly, the EPBs were developed even prior to the apex sunset during these days. Later, during 10–12 April when the TC center moved further southeastward away from equator, EPBs were observed around 30 min after the apex sunset with periodic nature. Even though the month of April is favorable for the development of EPBs over Southeast Asian longitudes, the EPBs observed on 8 and 9 April shows significant difference in the occurrence time (20 and 10 min prior to apex sunset during 8 and 9 April, respectively), intensity, and periodic nature. Therefore, in the present study, we focus mainly on the EPB development and the corresponding atmospheric, ionospheric background conditions on 8 and 9 April 2013 in more detail. It is to be noted that these 2 days were magnetically quiet with an average daily dst index of −6 and −4, respectively.

In order to further understand the spatial and temporal evolution of EPBs, we have analyzed the fan-sector backscatter maps obtained from the 16 beams of EAR. The onset and evolution of periodic EPBs observed on 8 April 2013 are shown in Figure 3. The green and red curves indicate the local and apex sunset terminators in altitude-zonal distance plane. The development of a fresh EPB can be seen at 1934 LT around 425 km altitude (red star) at the eastern edge of the fan-sector map and labeled as EPB-1 in Figure 3. As the sunset terminator moving westward, two more EPBs were freshly developed at 1938 LT around 425 km (635 km at apex) altitude in the center and western edge of fan-sector map (labeled as EPB-2 and EPB-3 in Figure 3). The red stars at 1938 LT shows the onset locations of all the three EPBs, which are freshly evolved over EAR. Interestingly, EPB-2 is developed around the apex sunset, and EPB-3 is started to develop just before the local sunset. As time progresses, all the three EPBs show a rapid growth and drifted eastward. From the analysis of fan-sector maps during the entire night of 8 April 2013, five more EPBs were also observed, and these EPBs were developed over the western longitudes of EAR and drifted in to the

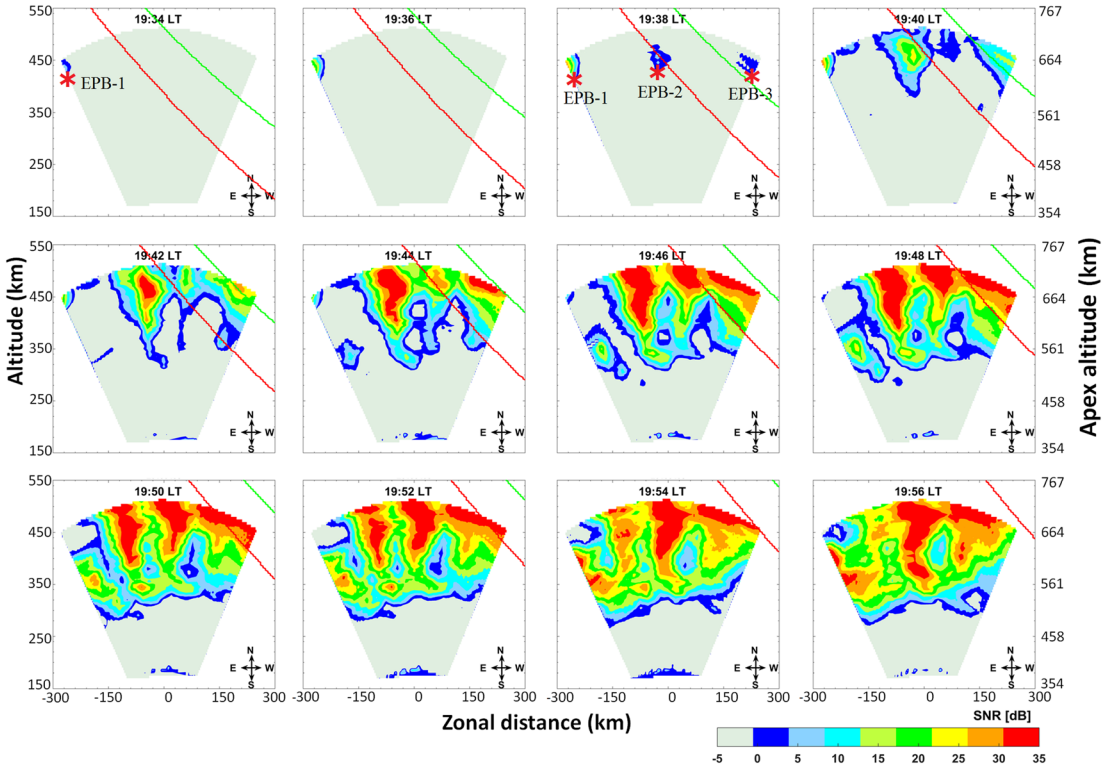

Figure 3. Fan-sector maps of backscatter echoes obtained from the 16 beams of EAR during 1934–1956 LT on 8 April 2013. The red star indicates the onset location of EPBs, and green and red curves indicate the local and apex sunset, respectively.

field of view (FoV) of EAR (not shown in Figure 3). These drifting-in EPBs can be observed in Figure 2e between 20 and 24 LT.

Similarly, the onset and successive development of EPBs during 9 April 2013 also analyzed using the fan-sector maps, and all the fresh and periodic EPBs observed around sunset hours of 8 and 9 April 2013 are summarized in Figure 4. The dotted magenta lines indicate the beam directions of EAR, and red stars

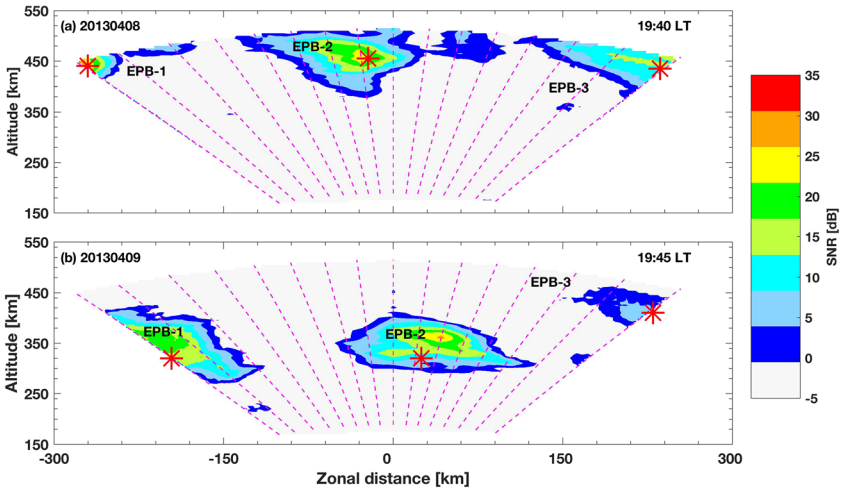

Figure 4. Fan sector maps of backscatter echoes observed from EAR during (a) 19:40 LT on 8 April 2013 and (b) 19:45 LT on 9 April 2013. The dotted magenta lines represent the 16 beam directions of EAR, and red stars indicate the onset locations of each EPB.

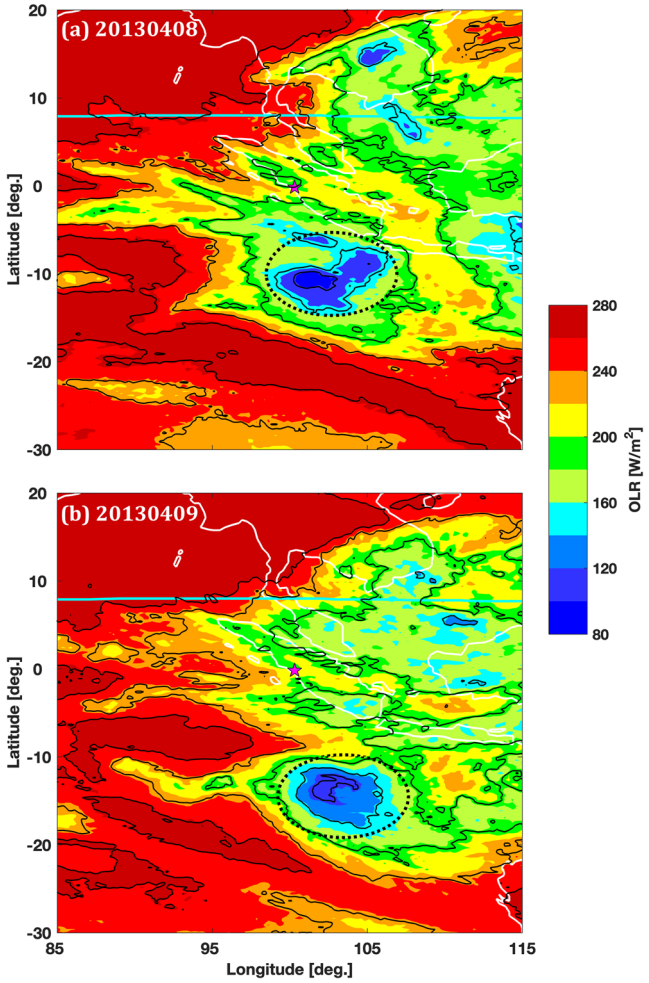

Figure 5. The longitudinal and latitudinal distribution of outgoing long-wave radiation (OLR) on (a) 8 and (b) 9 April 2013 as derived from VHRR on-board Indian meteorological satellite (Kalpana-1) over Indian and Indonesian region. The black dotted circle indicates the deep convective region due to TC Victoria. The magenta star and cyan horizontal line represents the EAR location and magnetic equator, respectively.

represent the onset location of each EPBs. It can be seen from Figure 4 that during the postsunset hours of 8 and 9 April 2013, daily three periodic EPBs were observed (labeled as EPB-1, EPB-2, and EPB-3) within the FoV of EAR. The EPBs observed on 8 and 9 April 2013 are separated by a zonal distance of 248, 258, 221, and 205 km respectively with an average inter-bubble distance of ~250 km. Further, from the observation of temporal variation of EPBs with respect to zonal distance using the 16 beams of EAR, the zonal drift velocity is estimated as 157.9, 164.1, 142.3, and 159.5 m/s for EPB-2 and EPB-3 on 8 and 9 April, respectively (Fukao et al., 2006). In addition to these fresh EPBs, several drifting-in EPBs also observed periodically at later times on these nights. However, in order to understand the possible seeding source of EPBs, in the present study, we only focused on the spatial and temporal evolution of the freshly evolved periodic EPBs within the FoV of EAR.

With a view to further understand the background atmospheric conditions responsible for the development of these periodic and intense EPBs, we have looked in to the convective activity for the possible seeding of EPBs by GWs. As we already discussed, the convective activities in the tropospheric region are one of the major source of GWs. The previous studies, which examined the correlation between atmospheric convection and EPB occurrence, have mainly used OLR values to detect the convective activity (e.g., McClure et al., 1998; Tsunoda, 2010). Similarly, here we use the daily averaged OLR data with spatial resolution of 0.25 × 0.25° from the VHRR instrument onboard Kalpana-1 satellite to explore the presence of convective activity (Singh et al., 2007). The OLR values obtained during 8 and 9 April 2013 over Indonesian region are plotted as a function of latitude and longitude in Figure 5. The cyan horizontal line represents the geomagnetic equator, and EAR location is shown in magenta star. Generally, the OLR values below 230 Wm^{-2} are considered as the presence of convective activity and above which it is nonconvective (Tsunoda, 2010; Waliser et al., 1993). From Figure 5a, the presence of a deep convective activity can be observed in the South Indian Ocean with OLR value of ~100 Wm^{-2} centered around 9.2°S, 101.6°E in association with the TC Victoria (marked by black dotted circle). On 9 April (Figure 5b), the cyclone center is moved toward southeast direction and reached around 11.4°S, 102.5°E. During 8 and 9 April, the deep convective region due to TC Victoria is located close to EAR location as well as magnetic equator (~8°N geog. lat).

Now, in effort to examine the presence of upward propagating GWs from this deep convective region, the vertical temperature profiles obtained from GPS-RO measurements at an altitude range of 10–40 km were filtered using a high pass fourth-order Butter-worth filter with a cut-off at 7 km (Ming et al., 2019). Figures 6a and 6d show the geographic locations of three available GPS-RO soundings close to TC Victoria superimposed on the half hourly averaged brightness temperature at 11 UT on 8 and 9 April, respectively. The corresponding temperature and temperature perturbation profiles as a function of altitude are shown in Figures 6b, 6c, 6e, and 6f. Temperature perturbations with amplitude greater than 1 K were observed in all the profiles during 8 and 9 April. By applying the fast Fourier transform (FFT) to the temperature perturbations the dominant vertical wavelengths of GW signature were estimated as 4.9 km (8 April) and 6 km (9 April).

In order to understand the possible seeding mechanism on the development of these periodic EPBs, we have examined the presence of GWs in the ionospheric altitudes during 8 and 9 April 2013. The upward propagating GWs result wave-like modulations in the *F* layer plasma, and it can be observed as quasi periodic oscillations in bottom side *F* layer virtual height (h'F) (Klausner et al., 2009; Rottger, 1977). Figure 7 shows the temporal variations in the fixed frequency (5–9 MHz) virtual height (h'F) (top panel) and virtual height

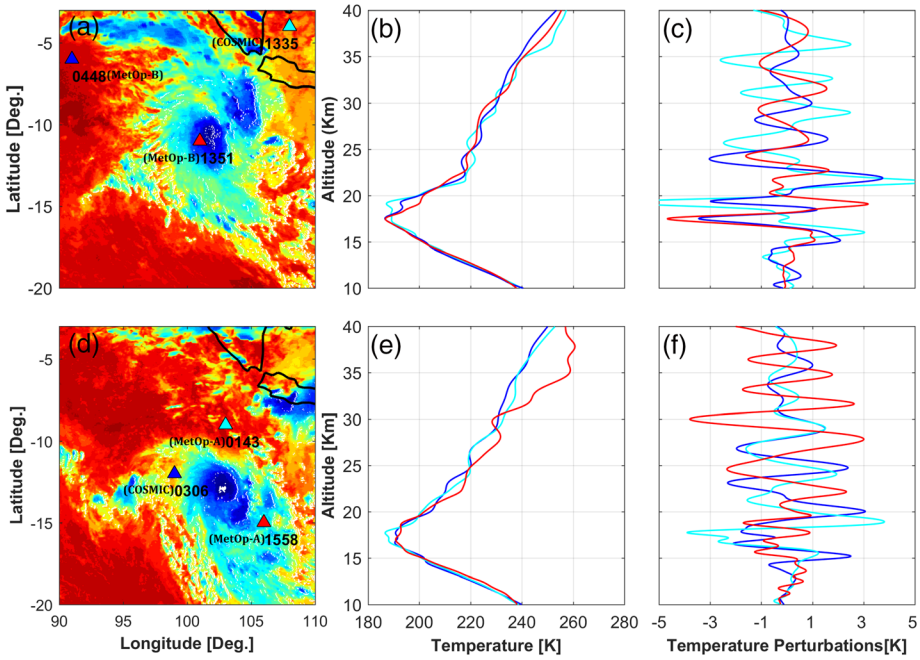

Figure 6. The geographic locations of three available GPS RO soundings close to TC Victoria superimposed on the half hourly averaged brightness temperature at 11 UT on (a and d) 8 and 9 April. The (b and e) corresponding temperature and (c and f) temperature perturbation profiles are given as a function of altitude. The different colors of triangles indicate the different sounding locations and the same colors used for the corresponding temperature profiles.

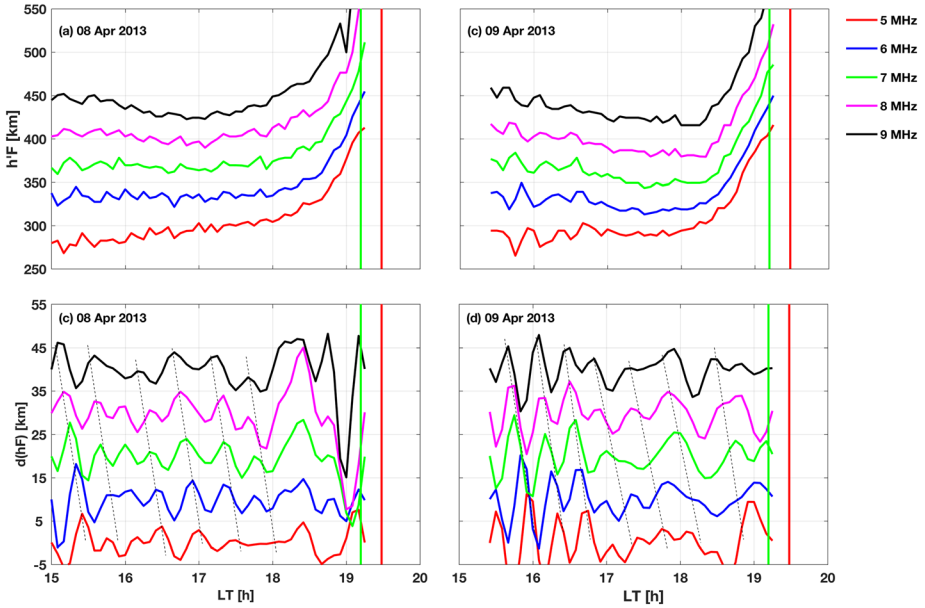

Figure 7. Temporal variations in the fixed frequency (5–9 MHz) virtual heights (h'F) (upper panel) and virtual height deviations (dh'F, band-pass filtered between 20 and 90 min) (lower panel) observed at Chumphon during 15–20 LT on 8 and 9 April 2013. The black dotted lines indicate the downward phase propagation of GW. The green and red lines indicate the *E* region and *F* region sunset over Chumphon.

Table 2
Upward Propagating GW Parameters Estimated Using the h'F Isofrequency Lines from Chumphon Ionosonde

Date	Vertical phase speed (m/s)	Observed time period (min)	Vertical wavelength (km)
8 April 2013	118.05	24.6	174.2
9 April 2013	120.5	24.7	178.5

deviation (dh'F) (bottom panel) observed at near equatorial station Chumphon (which is located along approximately same longitude of EAR) during the afternoon to evening period of 8 and 9 April 2013. Different colors in Figure 7 indicate the h'F and dh'F observation at frequencies ranges from 5 to 9 MHz with 1-MHz interval. The band pass filtered virtual height variation is plotted with a shift of 5 km (cumulative) for each frequency. One can clearly observe that the peaks appear earlier at higher frequencies compared to lower frequencies, indicating clear downward phase propagation. This is a typical characteristic of upward propagating atmospheric GWs (Abdu et al., 2009; Klausner et al., 2009; Takahashi et al., 2018). The period (T) of observed GW is estimated using the Lomb-Scargle periodogram analysis of the isofrequency lines of dh'F with 6 and 7 MHz. The vertical phase speed (V_Z) can be estimated using the virtual height (h'F) and time of two nearby frequencies (6 and 7 MHz used in the present study) using the following equation:

$$V_Z = \frac{h_{f2} - h_{f1}}{t_{f2} - t_{f1}}$$

where h_{f1} and h_{f2} and t_{f1} and t_{f2} are the virtual heights and corresponding time at frequencies $f1$ and $f2$, respectively. Finally, the vertical wavelength (λ_Z) can be estimated using the relation $\lambda_Z = V_Z \times T$ (Klausner et al., 2009). Using the above equations, the period, vertical wavelength and vertical velocity of the observed GWs during 8 and 9 April 2013 were estimated and listed in Table 2. These values are in good agreement with the earlier observations at ionospheric altitudes (see, e.g., Klausner et al., 2009; Vadas, 2007).

4. Discussion

The EAR observations presented in Figures 2, 3, and 4 evidently confirm the occurrence of intense and periodic presunset EPBs during two consecutive nights of 8 and 9 April 2013. Further, from Figures 3 and 4, one can observe the freshly evolved periodic EPBs that are separated by a zonal distance of ~250 km. By analyzing 3 years of data collected by an airglow imaging system located at Chile, Makela et al. (2010) estimated the spacing between periodic EPBs and showed that the bubble spacing distribution peaks around 200–300 km. Further, Sun et al. (2016) estimated the distance between adjacent EPBs using a network of four airglow imagers in the Chinese longitudes during 2012–2014, and the average distance is reported as 200–300 km. They attributed this periodic spacing of EPBs to the periodic GWs generated from deep convection activity at lower atmosphere. The interbubble distance (~250 km) obtained from the present study also corroborates with the above-mentioned periodic EPB observations.

To further investigate the presence and propagation characteristics of GWs at ionospheric altitudes, the 30-s GPS-VTEC data obtained from the 16 stations close to EAR (listed in Table 1) were subjected to a band pass filter with pass band frequency of 0.6–1 MHz using a second-order Butterworth filter. Only the VTEC data with elevation angle greater than 15° are considered. The observed VTEC perturbations (TECPs) show a clear wave like pattern of ~20-min period in more than one satellite from all the 16 stations. The observed periodicity of the wave patterns in VTEC perturbations appears to be that of typical atmospheric GWs. The VTEC variation from PRN 23, which was passing over the magnetic equatorial region, EAR location, and cyclone center, is plotted as a function of time in Figures 8a and 8b (top panels). The corresponding filtered VTEC is plotted as a function of UT and horizontal distance from cyclone center during 8 and 9 April 2013 in Figures 8c and 8d (bottom panels). From Figures 8c and 8d, one can observe clear GW patterns with significant amplitude during the evening hours of 8 and 9 April 2013. The IPP trajectories of PRN 23 during 8 and 9 April 2013 from 9.5 to 13.5 UT are shown in the inset plots of Figures 8c and 8d. The red star indicates the cyclone center, and blue dot represents the EAR location. It should be noted that the IPP was passing from dip equator to southeastward direction toward EAR location and cyclone center during this period. The magenta stars in Figure 8 indicate the sunset terminator at IPP altitude (350 km) for each station. Similar to the EAR observation, it can be seen from Figures 8c and 8d that ionospheric irregularities (observed as large amplitude TEC fluctuations) start to develop prior to the apex sunset during 8 and 9 April 2013. Further, a clear horizontal propagation of the GW fronts can be observed during the presunset

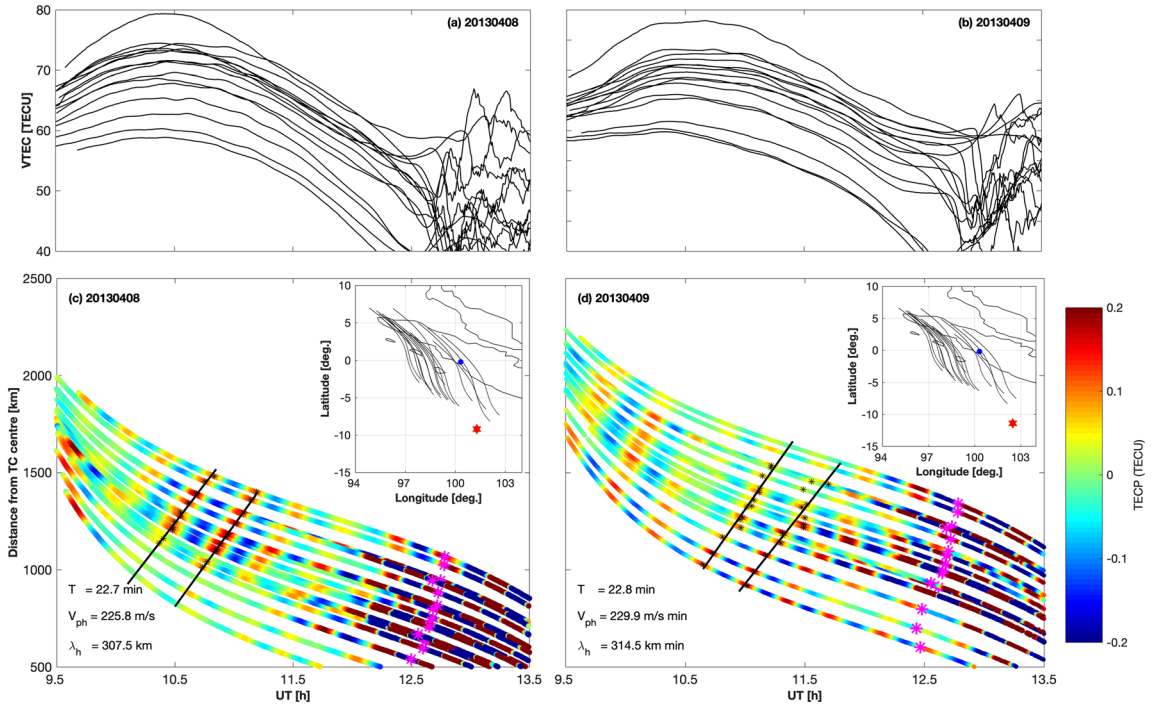

Figure 8. The VTEC observations from 16 GPS stations used in the present study as a function of UT (upper panel). Travel time diagram constructed using the band pass filtered TEC data obtained from PRN 23 for the 16 GPS stations close to EAR location during (c) 8 and (d) 9 April 2013. The magenta stars indicate the sunset terminator at IPP altitude (350 km) for each station. The inset plots show the IPP trajectories of PRN 23 for the 16 stations used in this study. The blue dot and red star in the inset plot represent the EAR location and cyclone center, respectively.

sector from Figure 8. The horizontal phase velocity (V_{ph}) is calculated by averaging the slope of linear fit (represented by the black lines in Figures 8c and 8d) of the two consecutive phase fronts of VTEC perturbations. The time period T is calculated using the Lomb-Scargle periodagram of TEC perturbations of individual stations and averaging at the end. Finally, the horizontal wavelength (λ_h) is estimated from the relation, $\lambda_h = T \times V_{ph}$ (Song et al., 2017, 2019). The time period and horizontal velocity deduced for 8 and 9 April are ~23 min, ~225 m/s and ~23 min, ~230 m/s, respectively. The estimated horizontal wavelengths are ~307 and ~315 km during these days, and these wavelengths are consistent with the values obtained from the previous observational and modeling studies (e.g., Abdu et al., 2009; Takahashi et al., 2009; Vadas, 2007).

The observed horizontal wavelength of GW (~300 km) is almost in good agreement with the obtained interbubble distance of the periodic EPBs (~250 km); this further strengthens the possibility of GW seeding on the development of these EPBs during 8 and 9 April 2013. Quite a few attempts were made to estimate and compare the interbubble distance and wavelength of the background seeding sources such as GWs (Paulino et al., 2011; Takahashi et al., 2009; Taori et al., 2011) and MSTIDs (Takahashi et al., 2018; Taori et al., 2015). Most of these studies show a good agreement between the GW/MSTID wavelength with the interbubble distance. Especially, during SpreadFx campaign, Takahashi et al. (2009) have shown a good correlation between the horizontal wavelengths of mesospheric GWs and interbubble distance from OI 6300 airglow imager.

In the search for the possible source for the periodic seeding of EPBs, the OLR observations (Figure 5) elucidate the presence of a deep convective region centered on TC Victoria near the location of EAR. Further, the temperature perturbation extracted from the GPS-RO temperature profiles indicates the presence of upward propagating GWs from the deep convective region near to TC Victoria at atmospheric altitudes. In addition, the GW parameters extracted from the virtual height measurements (Figure 7) from the Chumphon Ionosonde data and GPS-VTEC observations (Figure 8) confirm the presence of GWs at ionospheric altitudes during these days. These results strengthen the plausible development of spatially

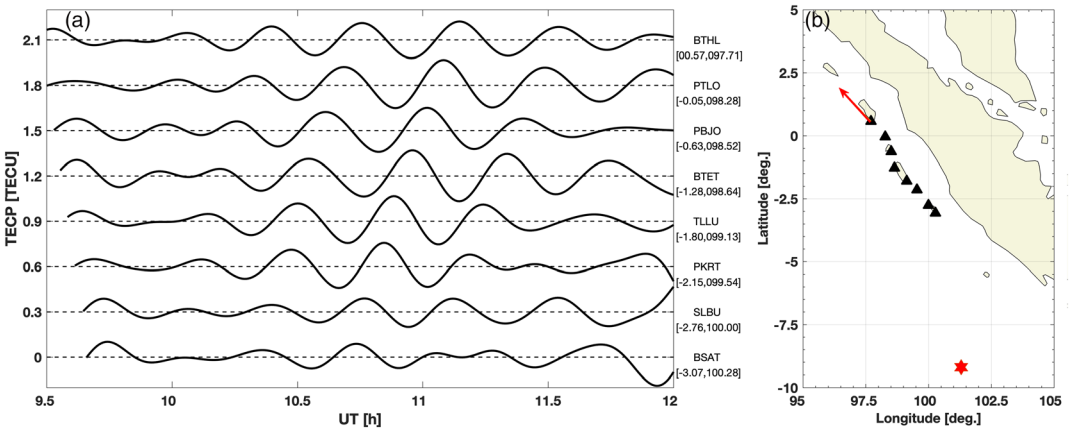

Figure 9. TEC perturbations observed by eight GPS receivers arranged in SE to NW direction from PRN 23 during 9.5–12 UT on 8 April 2013. The name and location of stations are shown in the right-hand side. The geographic locations of all the eight GPS stations are shown in the right panel as filled black triangles. The red filled star indicates the location of TC center. The red arrow represents the propagation direction of gravity wave front at BTHL obtained by SADM-GPS analysis using the three station array of BITI-BTHL-PTLO.

periodic EPBs via seeding of RT instability from the upward propagating GWs associated with TC Victoria. However, in the present study, the deep convective region due to TC Victoria during 8 and 9 April 2013 is 1,920 and 2,170 km away from the magnetic equator. This distance increases in the subsequent days as the cyclone center moves toward southeast direction. Hence, in order to seed the EPBs, the GWs should reach the bottom side ionosphere over magnetic equator. As we already mentioned in the introduction, this can be possible either by the direct propagation of GWs from TC center to ionospheric altitudes without any dissipation or by the secondary GWs generated by the dissipation of primary GWs at middle atmosphere. The GW observations from GPS-RO on 8 and 9 April (Figures 6c and 6f) show that the GW amplitude is saturated around 30 km and after that it is decreasing with altitude. The amplitude of nondissipating GWs is expected to increase exponentially with altitude (Hines, 1960). Hence, the observed GWs might have dissipated at middle atmospheric altitudes. Moreover, the vertical wavelength of GWs derived from GPS-RO observations are less than 6 km and with this vertical wavelength the direct propagation of GW to the bottom side *F* layer is not possible (Vadas, 2007; Vadas & Nicolls, 2012). Therefore, the observed GWs at ionospheric altitudes might be the secondary GWs generated in the middle atmosphere by the dissipation of primary GWs associated with TC Victoria. Similar to the present study, Vadas and Crowley (2010) have been observed the GWs at ionospheric altitudes using TIDDBIT ionospheric sounder associated with a tropical storm (TS Noel) located around 15° south of the sounder. They have reported that the observed GWs at ionospheric altitudes with $\lambda_h > 235$ km and $V_{ph} > 205$ m/s cannot be generated from convective activity at lower atmosphere; instead, those waves are secondary GWs generated by the dissipation of primary GWs (associated with TS Noel) at middle atmosphere. One can observe that the λ_h and V_{ph} of GWs obtained in the present study are ~300 km and 225 m/s, respectively. This further confirms that the GWs observed at the ionospheric altitudes in the present study are secondary GWs possibly generated due to TC Victoria and not the primary GWs directly propagated from the TC center.

With a view to further understand the propagation direction of GWs observed at ionospheric altitudes by GPS VTEC observations, the GPS stations were arranged in the SE to NW direction, and TEC perturbations from individual stations were plotted in Figure 9 as a function of UT (Valladares et al., 2015). Similar to Figure 8, the TEC perturbations were derived using the VTEC values obtained from PRN 23. The name and coordinates of each station are shown in the right hand side of Figure 9a, and the geographic locations are represented as black triangles in Figure 9b. One can observe that the TEC perturbations appear at earlier times at stations that are situated southeast compared to the northwest stations. Hence, it can be understood that the GWs observed on 8 April 2013 over Indonesian longitudes are propagating either northward or northwestward. Similar propagation characteristics were observed on 9 April 2013 also (not shown in figure). In order to confirm the exact propagation direction of GW fronts, we have used the statistical

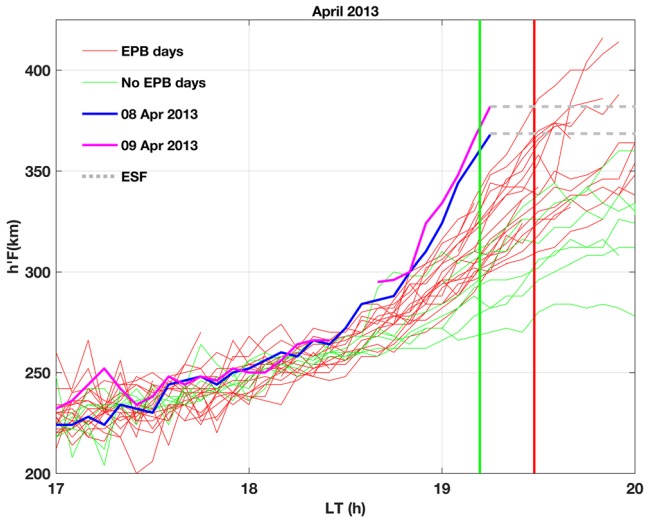

Figure 10. The *F* layer virtual height (h'F) variation over the equatorial station Chumphon for the month of April 2013. The green and red lines indicate the *E* region and *F* region sunset over Chumphon. The dotted gray lines represent equatorial spread *F* (ESF).

angle of arrival and Doppler method for GPS radio interferometry (SADM-GPS) technique developed by Afraimovich et al. (1998). This method uses TEC perturbations from a GPS array that consists of three stations which are spaced in an assumed *x-y* plane with distance less than one half of the wavelength of TEC perturbation (Afraimovich et al., 2003). Further, it is assumed that all the three GPS receivers observe same perturbations in the TEC data. The detailed description of the SADM-GPS technique can be seen in the work of Afraimovich et al. (1998), Habarulema et al. (2013), and Valladares and Hei (2012). In the present study, we have used the closely spaced stations BITI, BTHL, and PTLO for the estimation of direction of GW fronts at the reference station BTHL. The propagation direction of GW front at BTHL station is estimated as −43.25° and −42.18° from the north on 8 and 9 April, respectively. The red arrow in Figure 9 (right panel) represents the propagation direction of GW front at BTHL on 8 April. Thus, the results obtained from SADM-GPS technique and the phase difference observed in TEC perturbations (Figure 9) confirm the propagation of GWs to magnetic equatorial region in the northwest direction with respect to the TC location.

Another interesting observation in the present study is the onset of pre-sunset EPBs. One can observe from Figures 2 and 3 that the EPBs during 8 and 9 April 2013 show the development prior to the apex sunset. Interestingly, on 8 April 2013, the onset of EPB occurred around the local sunset (Figure 3). Usually, the majority of freshly evolving EPBs observed from EAR are found to occur around or within 1 hr from the apex sunset (Ajith et al., 2015, 2016; Yokoyama et al., 2004). Hence, in order to examine the background ionospheric conditions, the bottomside *F* layer virtual height variation (h'F) were estimated using the ionosonde located in the low-latitude station Chumphon. Figure 10 shows the variation of h'F over Chumphon during the month of April 2013. The red and green curves indicate the h'F during EPB days and non-EPB days. The blue and magenta curves show the h'F during 8 and 9 April 2013, respectively. The green and red vertical line in Figure 10 indicates the *E* region (100 km) and *F* region (200 km) sunset over Chumphon. One can clearly see from Figure 10 that around *E* region sunset h'F is significantly high during 8 and 9 April 2013. The augmented electric field associated with GWs may results the elevation of *F* layer to higher altitudes even prior to the *E* region sunset during these days, where the cyclone center was closer to the equatorial region as compared to other days. Once the GWs reached the ionospheric altitudes, the vertical component of GW wind (U_Z) can build up zonal polarization electric field by the relation $E_y = -\Delta U_Z \times B_0$, where B_0 is the Earth's magnetic field (Abdu et al., 2009, 2015). There are several reports, which confirm the development and enhancement of electric field during TCs/tropical typhoons (Bishop et al., 2006; Isaev et al., 2010; Sorokin et al., 2005). Similar to the presunset EPB observation by EAR and GPS-TEC, the ionosonde observations also show the presence of ESF irregularities prior to the apex sunset during 8 and 9 April 2013 (gray dotted line in Figure 10). There are several studies, which confirmed the amplification of *F* layer bottomside wave structure and associated polarization electric field prior to the *E* region sunset (Abdu et al., 2015; Thampi et al., 2009; Tulasi Ram et al., 2014).

5. Conclusion

Interesting development of periodic and intense EPBs prior to the apex sunset during two consecutive nights on 8 and 9 April 2013 was observed by the 47-MHz EAR over Indonesian longitudes. The freshly evolved EPBs with interbubble distance of ~250 km were detected in the FoV of EAR during this period. In the present study, we have examined the possible background atmospheric and ionospheric conditions for the development of these periodic and intense EPBs using multi-instrumental observations such as GPS-TEC, OLR, GPS RO, VHF radar, and Ionosonde. The presence of a deep convective activity close to the EAR location was observed during these periods due to the occurrence of a TC named TC Victoria. The presence of GWs associated with this deep convective region at atmospheric and ionospheric altitudes were confirmed by the temperature perturbations obtained from GPS-RO observations and downward phase propagation of small amplitude oscillations in the *F* layer bottom height isofrequency measurements obtained from

Chumphon Ionosonde. The propagation characteristics and the horizontal wavelength of GWs are estimated using the GPS-TEC observations from the stations close to the EAR location and magnetic equator. The obtained wave parameters confirm the presence of GW activity close to the geomagnetic equator with horizontal wavelength of ~300 km. The estimated wavelength is close to the interbubble distance of periodic EPBs observed during this period. The GW parameters observed from GPS-TEC and GPS-RO show the possible development of secondary GWs from the dissipation of primary GWs associated with TC Victoria at middle atmosphere. Further, the estimated propagation direction of GW fronts indicates the NW propagation of GWs with respect to TC location. By considering all the above findings, it can be argued that the GWs associated with TC Victoria might have resulted the initial seed perturbation for the development of these periodic EPBs. Additionally, the observation from EAR, Chumphon Ionosonde, and GPS-TEC shows the development of EPBs prior to the apex sunset during 8 and 9 April 2013. The cyclone center was close to geomagnetic equator, and *F* layer was elevated to higher altitudes before sunset during these days. The polarization electric fields associated with GWs may results the uplift of *F* layer and further development of pre-sunset EPBs during these days.

Data Availability Statement

The EAR data can be obtained online (http://www.rish.kyoto-u.ac.jp/ear/index-e.html). The CPN ionosonde data are available under SEALION network (http://seg-web.nict.go.jp/sealion/). The 4-km resolution brightness temperature data are available from NASA Goddard Earth Sciences Data and Information Services Center (GES DISC) (https://disc.gsfc.nasa.gov/datasets/GPM_MERGIR_1/summary). SuGAr GPS data can be downloaded online (http://sopac.ucsd.edu). The GPS radio occultation profiles of COSMIC, MetOp-A, and MetOp-B satellites can be obtained from UCAR-CDAAC (https://cdaac-www.cosmic.ucar.edu/cdaac/ tar/rest.html).

Acknowledgments

The work was partly supported by the National Natural Science Foundation of China (42020104002 and 41727803) and the Postdoctoral Fellowship at Institute of Geology and Geophysics, Chinese Academy of Sciences (IGGCAS). We thank Priyesh Kunnummal for extending his help during the formulation of this paper. We acknowledge Indian Institute of Tropical Meteorology (IITM) Pune for providing the 3 hourly averaged OLR values from VHRR onboard Kalapana-1 satellite (https://tropmet.res.in/static_pages.php?page_id = 144).

References

Aarons, J. (1982). Global morphology of ionospheric scintillations. *Proceedings of the IEEE*, *70*, 360–378.

Abdu, M. A., Alam Kherani, E., Batista, I. S., de Paula, E. R., Fritts, D. C., & Sobral, J. H. A. (2009). Gravity wave initiation of equatorial spread *F*/plasma bubble irregularities based on observational data from the SpreadFEx campaign. *Annales de Geophysique*, *27*(7), 2607–2622. https://doi.org/10.5194/angeo-27-2607-2009

Abdu, M. A., Bittencourt, J. A., & Batista, I. S. (1981). Magnetic declination control of the equatorial F region dynamo electric field development and spread *F*. *Journal of Geophysical Research*, *86*(A13), 11,443–11,446. https://doi.org/10.1029/JA086iA13p11443

Abdu, M. A., De Medeiros, R. T., & Sobral, J. H. A. (1982). Equatorial spread *F* instability conditions as determined from ionograms. *Geophysical Research Letters*, *9*(692), 692–695. https://doi.org/10.1029/GL009i006p00692

Abdu, M. A., de Souza, J. R., Kherani, E. A., Batista, I. S., MacDougall, J. W., & Sobral, J. H. A. (2015). Wave structure and polarization electric field development in the bottomside *F* layer leading to postsunset equatorial spread *F*. *Journal of Geophysical Research: Space Physics*, *120*, 6930–6940. https://doi.org/10.1002/2015JA021235

Afraimovich, E. L., Palamartchouk, K. S., & Perevalova, N. P. (1998). GPS radio interferometry of travelling ionospheric disturbances. *Journal of Atmospheric and Solar - Terrestrial Physics*, *60*(12), 1205–1223. https://doi.org/10.1016/S1364-6826(98)00074-1

Afraimovich, E. L., Perevalova, N. P., & Voyeikov, S. V. (2003). Traveling wave packets of total electron content disturbances as deduced from global GPS network data. *Journal of Atmospheric and Solar - Terrestrial Physics*, *65*(11–13), 1245–1262. https://doi.org/10.1016/j.jastp.2003.08.007

Ajith, K. K., Tulasi Ram, S., Carter, B. A., Sathish Kumar, S., Yamamoto, M., Yokoyama, T., et al. (2018). Unseasonal development of post-sunset *F*-region irregularities over Southeast Asia on 28 July 2014: 2. Forcing from below? *Progress in Earth and Planetary Science*, *5*, 60. https://doi.org/10.1186/s40645-018-0218-1

Ajith, K. K., Tulasi Ram, S., Yamamoto, M., Otsuka, Y., & Niranjan, K. (2016). On the fresh development of equatorial plasma bubbles around the midnight hours of June solstice. *Journal of Geophysical Research: Space Physics*, *121*, 9051–9062. https://doi.org/10.1002/2016JA023024

Ajith, K. K., Tulasi Ram, S., Yamamoto, M., Yokoyama, T., Gowtam, V. S., Otsuka, Y., et al. (2015). Explicit characteristics of evolutionary-type plasma bubbles observed from Equatorial Atmosphere Radar during the low to moderate solar activity years 2010–2012. *Journal of Geophysical Research: Space Physics*, *120*, 1371–1382. https://doi.org/10.1002/2014JA020878

Basu, S., MacKenzie, E., & Basu, S. (1988). Ionospheric constraints on VHF/UHF communications links during solar maximum and minimum periods. *Radio Science*, *23*, 363–378. https://doi.org/10.1029/RS023i003p00363

Bauer, S. J. (1958). An apparent ionospheric response to the passage of hurricanes. *Journal of Geophysical Research*, *63*(1), 265–269. https://doi.org/10.1029/JZ063i001p00265

Bishop, R. L., Aponte, N., Earle, G. D., Sulzer, M., Larsen, M. F., & Peng, G. S. (2006). Arecibo observations of ionospheric perturbations associated with the passage of Tropical Storm Odette. *Journal of Geophysical Research*, *111*, A11320. https://doi.org/10.1029/2006JA011668

Buonsanto, M. J. (1999). Ionospheric storms—A review. *Space Science Reviews*, *88*(3/4), 563–601. https://doi.org/10.1023/A:1005107532631

Carter, B. A., Tulasi Ram, S., Yizengaw, E., Pradipta, R., Retterer, J., Norman, R., et al. (2018). Unseasonal development of *F*-region irregularities over Southeast Asia on 28 July 2014. *Progress in Earth and Planetary Science*, *5*, 10. https://doi.org/10.1186/s40645-018-0164-y

Ding, F., Wan, W., Xu, G., Yu, T., Yang, G., & Wang, J. (2011). Climatology of medium-scale traveling ionospheric disturbances observed by a GPS network in central China. *Journal of Geophysical Research*, *116*, A09327. https://doi.org/10.1029/2011JA016545

Farley, D. T., Bonelli, E., Fejer, B. G., & Larsen, M. F. (1986). The prereversal enhancement of the zonal electric field in the equatorial ionosphere. *Journal of Geophysical Research*, *91*(A12), 13,723–13,728. https://doi.org/10.1029/JA091iA12p13723

Fejer, B. G., de Paula, E. R., Gonzalez, S. A., & Woodman, R. F. (1991). Average vertical and zonal *F* region plasma drifts over Jicamarca. *Journal of Geophysical Research*, *96*(A8), 13,901–13,906. https://doi.org/10.1029/91JA01171

Fritts, D. C., Abdu, M. A., Batista, B. R., Batista, I. S., Batista, P. P., Buriti, R., et al. (2009). Overview and summary of the Spread *F* Experiment (SpreadFEx). *Annales de Geophysique*, *27*(5), 2141–2155. https://doi.org/10.5194/angeo-27-2141-2009

Fritts, D. C., & Alexander, M. J. (2003). Gravity wave dynamics and effects in the middle atmosphere. *Reviews of Geophysics*, *41*, 1003. https://doi.org/10.1029/2001RG000106

Fritts, D. C., & Nastrom, G. D. (1992). Sources of mesoscale variability of gravity waves, II, frontal, convective, and jet stream excitation. *Journal of the Atmospheric Sciences*, *49*(2), 111–127. https://doi.org/10.1175/1520-0469(1992)049<0111:SOMVOG>2.0.CO;2

Fukao, S., Hashiguchi, H., Yamamoto, M., Tsuda, T., Nakamura, T., Yamamoto, M. K., et al. (2003). Equatorial Atmosphere Radar (EAR): System description and first results. *Radio Science*, *38*(3), 1053. https://doi.org/10.1029/2002RS002767

Fukao, S., Yokoyama, T., Tayama, T., Yamamoto, M., Maruyama, T., & Saito, S. (2006). Eastward traverse of equatorial plasma plumes observed with the Equatorial Atmosphere Radar in Indonesia. *Annales de Geophysique*, *24*(5), 1411–1418. https://doi.org/10.5194/angeo-24-1411-2006

Habarulema, J. B., Katamzi, Z. T., & McKinnell, L.-A. (2013). Estimating the propagation characteristics of large-scale traveling ionospheric disturbances using ground-based and satellite data. *Journal of Geophysical Research: Space Physics*, *118*, 7768–7782. https://doi.org/10.1002/2013JA018997

Haerendel, G. (1973). Theory of equatorial spread *F*, report, Max-Planck Inst. for Phys., and Astrophys, Garching, Germany

Hines, C. O. (1960). Internal gravity waves at ionospheric heights. *Canadian Journal of Physics*, *38*(11), 1441–1481. https://doi.org/10.1139/p60-150

Huang, C.-S., de La Beaujardie`re, O., Roddy, P. A., Hunton, D. E., Ballenthin, J. O., Hairston, M. R., & Pfaff, R. F. (2013). Large-scale quasiperiodic plasma bubbles: C/NOFS observations and causal mechanism. *Journal of Geophysical Research: Space Physics*, *118*, 3602–3612. https://doi.org/10.1002/jgra.50338

Huang, C. S., & Kelley, M. C. (1996). Nonlinear evolution of equatorial spread *F*: 1. On the role of plasma instabilities and spatial resonance associated with gravity wave seeding. *Journal of Geophysical Research*, *101*(A1), 283–292. https://doi.org/10.1029/95JA02211

Hung, R. J., & Kao, J. P. (1978). Ionospheric observation of gravity waves associated with Hurricane Eloise. *Journal of Geophysics*, *45*, 67–80.

Hung, R. J., & Smith, R. E. (1978). Ray tracing of gravity waves as a possible warning system for tornadic storms and hurricanes. *Journal of Applied Meteorology*, *17*(1), 3–11. https://doi.org/10.1175/1520-0450(1978)017%3c0003:RTOGWA%3e2.0.CO;2

Hysell, D. L., Kelley, M. C., Swartz, W. E., & Woodman, R. F. (1990). Seeding and layering of equatorial spread *F* by gravity waves. *Journal of Geophysical Research*, *95*(A10), 17,253–17,260. https://doi.org/10.1029/JA095iA10p17253

Isaev, N. V., Kostin, V. M., Belyaev, G. G., Ovcharenko, O. Y., & Trushkina, E. P. (2010). Disturbances of the topside ionosphere caused by typhoons. *Geomagnetism and Aeronomy*, *50*(2), 243–255. https://doi.org/10.1134/S001679321002012X

Janowiak, J., Joyce, B., & Xie, P. P. (2017). In). In A. Savtchenko (Ed.), *NCEP/CPC L3 Half Hourly 4km Global (60S – 60N) Merged IR V1*. Greenbelt, MD: Goddard Earth Sciences Data and Information Services Center (GES DISC), Accessed: [*04-May-2020*]. https://doi.org/10.5067/P4HZB9N27EKU

Ke, F., Wang, J., Tu, M., Wang, X., Wang, X., Zhao, X., & Deng, J. (2019). Characteristics and coupling mechanism of GPS ionospheric scintillation responses to the tropical cyclones in Australia. *GPS Solutions*, *23*(2), 1, 34–14. https://doi.org/10.1007/s10291-019-0826-2

Kelley, M. C., LaBelle, J., Kudeki, E., Fejer, B. G., Basu, S. A., Basu, S., et al. (1986). The Condor equatorial spread *F* campaign: Overview of results of the large-scale measurements. *Journal of Geophysical Research*, *91*(A5), 5487. https://doi.org/10.1029/JA091iA05P05487

Kelley, M. C., Larsen, M. F., LaHoz, C., & McClure, J. P. (1981). Gravity wave initiation of equatorial spread *F*: A case study. *Journal of Geophysical Research*, *86*(A11), 9087. https://doi.org/10.1029/JA086iA11p09087

Klausner, V., Fagundes, P. R., Sahai, Y., Wrasse, C. M., Pillat, V. G., & Becker-Guedes, F. (2009). Observations of GW/TID oscillations in the *F*2 layer at low latitude during high and low solar activity, geomagnetic quiet and disturbed periods. *Journal of Geophysical Research*, *114*, A02313. https://doi.org/10.1029/2008JA013448

Klostermeyer, J. (1978). Nonlinear investigation of the spatial resonance effect in the nighttime equatorial *F* region. *Journal of Geophysical Research*, *83*, 3753–3760. https://doi.org/10.1029/JA083iA08P03753

Krall, J., Huba, J. D., & Fritts, D. C. (2013). On the seeding of equatorial spread *F* by gravity waves. *Geophysical Research Letters*, *40*, 661–664. https://doi.org/10.1002/GRL.50144

Li, G., Ning, B., Abdu, M. A., Otsuka, Y., Yokoyama, T., Yamamoto, M., & Liu, L. (2013). Longitudinal characteristics of spread *F* backscatter plumes observed with the EAR and Sanya VHF radar in Southeast Asia. *Journal of Geophysical Research: Space Physics*, *118*, 6544–6557. https://doi.org/10.1002/jgra.50581

Li, G., Ning, B., Liu, L., Ren, Z., Lei, J., & Su, S.-Y. (2007). The correlation of longitudinal/seasonal variations of evening equatorial pre-reversal drift and of plasma bubbles. *Annales de Geophysique*, *25*, 2571–2578. https://doi.org/10.5194/angeo-25-2571-2007

Li, G., Otsuka, Y., Ning, B., Abdu, M. A., Yamamoto, M., Wan, W., et al. (2016). Enhanced ionospheric plasma bubble generation in more active ITCZ. *Geophysical Research Letters*, *43*, 2389–2395. https://doi.org/10.1002/2016GL068145

Lou, Y., Luo, X., Gu, S., Xiong, C., Song, Q., Chen, B., et al. (2019). Two typical ionospheric irregularities associated with the tropical cyclones Tembin (2012) and Hagibis (2014). *Journal of Geophysical Research: Space Physics*, *124*, 6237–6252. https://doi.org/10.1029/2019JA026861

Makela, J. J., Vadas, S. L., Muryanto, R., Duly, T., & Crowley, G. (2010). Periodic spacing between consecutive equatorial plasma bubbles. *Geophysical Research Letters*, *37*, L14103. https://doi.org/10.1029/2010GL043968

McClure, J. P., Singh, S., Bamgboye, D. K., Johnson, F. S., & Kil, H. (1998). Occurrence of equatorial *F* region irregularities: Evidence for tropospheric seeding. *Journal of Geophysical Research*, *103*(A12), 29,119–29,135. https://doi.org/10.1029/98JA02749

Ming, F. C., Jolivet, S., Liou, Y. A., Jégou, F., Mekies, D., & Hong, J. S. (2019). Elliptical structures of gravity waves produced by Typhoon Soudelor in 2015 near Taiwan. *Atmosphere*, *10*, 260. https://doi.org/10.3390/atmos10050260

Nicolls, M. J., & Kelley, M. C. (2005). Strong evidence for gravity wave seeding of ionospheric plasma instability. *Geophysical Research Letters*, *32*, L05108. https://doi.org/10.1029/2004GL020737

Nishioka, M., Tsugawa, T., Kubota, M., & Ishii, M. (2013). Concentric waves and short-period oscillations observed in the ionosphere after the 2013 Moore EF5 tornado. *Geophysical Research Letters*, *40*, 5581–5586. https://doi.org/10.1002/2013GL057963

Otsuka, Y., Shiokawa, K., Ogawa, T., & Wilkinson, P. (2002). Geomagnetic conjugate observations of equatorial airglow depletions. *Geophysical Research Letters*, *29*(15), 1753. https://doi.org/10.1029/2002GL015347

Paulino, I., Takahashi, H., Medeiros, A. F., Wrasse, C. M., Buriti, R. A., Sobral, J. H. A., & Gobbi, D. (2011). Mesospheric gravity waves and ionospheric plasma bubbles observed during the COPEX campaign. *Journal of Atmospheric and Solar - Terrestrial Physics*, *73*(11–12), 1575–1580. https://doi.org/10.1016/j.jastp.2010.12.004

Rama Rao, P. V. S., Tulasi Ram, S., Niranjan, K., Prasad, D. S. V. V. D., Gopikrishna, S., & Lakshmi, N. K. M. (2005). VHF and L-band scintillation characteristics over Indian low-latitude station, Waltair. *Annales de Geophysique*, *23*(7), 2457–2464. https://doi.org/10.5194/angeo-23-2457-2005

Rottger, J. (1973). Wavelike structures of large scale equatorial spread *F* irregularities. *Journal of Atmospheric and Terrestrial Physics*, *35*(6), 1195–1206. https://doi.org/10.1016/0021-9169(73)90016-0

Rottger, J. (1977). Traveling disturbances in the equatorial ionospheric spread *F* and their association with penetrative cumulus convection. *Journal of Atmospheric and Terrestrial Physics*, *39*(9–10), 987–998. https://doi.org/10.1016/0021-9169(77)90007-1

Rottger, J. (1981). Equatorial spread *F* by electric fields and atmospheric gravity waves generated by thunderstorms. *Journal of Atmospheric and Terrestrial Physics*, *43*(5–6), 453–462. https://doi.org/10.1016/0021-9169(81)90108-2

Seemala, G. K. (2011). GPS-TEC analysis application, Tech. Rep., Inst. for Sci. Res., U.S.A.

Singh, R., Thapliyal, P. K., Kishtawal, C. M., Pal, P. K., & Joshi, P. C. (2007). A new technique for estimating outgoing longwave radiation using infrared window and water vapor radiances from Kalpana very high resolution radiometer. *Geophysical Research Letters*, *34*, L23815. https://doi.org/10.1029/2007GL031715

Singh, S., Johnson, F. S., & Power, R. A. (1997). Gravity wave seeding of equatorial plasma bubbles. *Journal of Geophysical Research*, *102*(A4), 7399–7410. https://doi.org/10.1029/96JA03998

Sivakandan, M., Paulino, I., Ramkumar, T. K., Taori, A., Patra, A. K., Sripathi, S., et al. (2019). Multi-instrument investigation of troposphere-ionosphere coupling and the role of gravity waves in the formation of equatorial plasma bubble. *Journal of Atmospheric and Solar - Terrestrial Physics*, *189*, 65–79. https://doi.org/10.1016/j.jastp.2019.04.006

Song, Q., Ding, F., Zhang, X., Liu, H., Mao, T., Zhao, X., & Wang, Y. (2019). Medium-scale traveling ionospheric disturbances induced by Typhoon Chan-hom over China. *Journal of Geophysical Research: Space Physics*, *124*, 2223–2237. https://doi.org/10.1029/2018JA026152

Song, Q., Ding, F., Zhang, X., & Mao, T. (2017). GPS detection of the ionospheric disturbances over China due to impacts of Typhoons Rammasum and Matmo. *Journal of Geophysical Research: Space Physics*, *122*, 1055–1063. https://doi.org/10.1002/2016JA023449

Sorokin, V. M., Isaev, N. V., Yaschenko, A. K., Chmyrev, V. M., & Hayakawa, M. (2005). Strong DC electric field formation in the low latitude ionosphere over typhoons. *Journal of Atmospheric and Solar - Terrestrial Physics*, *67*(14), 1269–1279. https://doi.org/10.1016/j.jastp.2005.06.014

Sun, L., Xu, J., Wang, W., Yuan, W., Li, Q., & Jiang, C. (2016). A statistical analysis of equatorial plasma bubble structures based on an all-sky airglow imager network in China. *Journal of Geophysical Research: Space Physics*, *121*, 11,495–11,517. https://doi.org/10.1002/2016JA022950

Takahashi, H., Taylor, M. J., Pautet, P.-D., Medeiros, A. F., Gobbi, D., Wrasse, C. M., et al. (2009). Simultaneous observation of ionospheric plasma bubbles and mesospheric gravity waves during the SpreadFEx campaign. *Annales de Geophysique*, *27*(4), 1477–1487. https://doi.org/10.5194/angeo-27-1477-2009

Takahashi, H., Wrasse, C. M., Figueiredo, C. A. O. B., Barros, D., Abdu, M. A., Otsuka, Y., & Shiokawa, K. (2018). Equatorial plasma bubble seeding by MSTIDs in the ionosphere. *Progress in Earth and Planetary Science*, *5*, 32. https://doi.org/10.1186/s40645-018-0189-2

Taori, A., Parihar, N., Ghodpage, R., Dashora, N., Sripathi, S., Kherani, E. A., & Patil, P. T. (2015). Probing the possible trigger mechanisms of an equatorial plasma bubble event based on multistation optical data. *Journal of Geophysical Research: Space Physics*, *120*, 8835–8847. https://doi.org/10.1002/2015JA021541

Taori, A., Patra, A. K., & Joshi, L. M. (2011). Gravity wave seeding of equatorial plasma bubbles: An investigation with simultaneous *F* region, *E* region, and middle atmospheric measurements. *Journal of Geophysical Research*, *116*, A05310. https://doi.org/10.1029/2010JA016229

Thampi, S. V., Yamamoto, M., Tsunoda, R. T., Otsuka, Y., Tsugawa, T., Uemoto, J., & Ishii, M. (2009). First observations of large-scale wave structure and equatorial spread *F* using CERTO radio beacon on the C/NOFS satellite. *Geophysical Research Letters*, *36*, L18111. https://doi.org/10.1029/2009GL039887

Tsunoda, R. T. (1985). Control of the seasonal and longitudinal occurrence of equatorial scintillations by the longitudinal gradient in integrated *E* region Pedersen conductivity. *Journal of Geophysical Research*, *90*, 447–456. https://doi.org/10.1029/JA090iA01p00447

Tsunoda, R. T. (2010). On equatorial spread *F*: Establishing a seeding hypothesis. *Journal of Geophysical Research*, *115*, A12303. https://doi.org/10.1029/2010JA015564

Tsunoda, R. T. (2015). Upwelling: A unit of disturbance in equatorial spread *F*. *Progress in Earth and Planetary Science*, *2*(1), 9. https://doi.org/10.1186/s40645-015-0038-5

Tsunoda, R. T., & White, B. R. (1981). On the generation and growth of equatorial backscatter plumes: 1. Wave structure in the bottomside *F* layer. *Journal of Geophysical Research*, *86*(A5), 3610–3616. https://doi.org/10.1029/JA086iA05p03610

Tulasi Ram, S., Rama Rao, P. V. S., Niranjan, K., Prasad, D. S. V. V. D., Sridharan, R., Devasia, C. V., & Ravindhran, S. (2006). The role of post sunset vertical drifts at the equator in predicting the onset of VHF scintillations during high and low sunspot activity years. *Annales de Geophysique*, *24*(6), 1609–1616. https://doi.org/10.5194/angeo-24-1609-2006

Tulasi Ram, S., Yamamoto, M., Tsunoda, R. T., Chau, H. D., Hoang, T. L., Damtie, B., et al. (2014). Characteristics of large-scale wave structure observed from African and Southeast Asian longitudinal sectors. *Journal of Geophysical Research: Space Physics*, *119*, 2288–2297. https://doi.org/10.1002/2013JA019712

Tulasi Ram, S., Yamamoto, M., Tsunoda, R. T., Thampi, S. V., & Gurubaran, S. (2012). On the application of differential phase measurements to study the zonal large scale wave structure (LSWS) in the ionospheric electron content. *Radio Science*, *47*, RS2001. https://doi.org/10.1029/2011RS004870

Vadas, S. L. (2007). Horizontal and vertical propagation and dissipation of gravity waves in the thermosphere from lower atmospheric and thermospheric sources. *Journal of Geophysical Research*, *112*, A06305. https://doi.org/10.1029/2006JA011845

Vadas, S. L., & Crowley, G. (2010). Sources of the traveling ionospheric disturbances observed by the ionospheric TIDDBIT sounder near Wallops Island on 30 October 2007. *Journal of Geophysical Research*, *115*, A07324. https://doi.org/10.1029/2009JA015053

Vadas, S. L., & Fritts, D. C. (2006). Influence of solar variability on gravity wave structure and dissipation in the thermosphere from tropospheric convection. *Journal of Geophysical Research*, *111*, A10S12. https://doi.org/10.1029/2005JA011510

Vadas, S. L., & Nicolls, M. J. (2012). The phases and amplitudes of gravity waves propagating and dissipating in the thermosphere: Theory. *Journal of Geophysical Research*, *117*, A05322. https://doi.org/10.1029/2011JA017426

Valladares, C. E., Carrano, C. S., Groves, K. M., Paznukhov, V. V., & Doherty, P. H. (2015). Forecasting the appearance and evolution of ionospheric irregularities and structures: Their effects on AF systems. AFRL-RV-PS- TR-2015-0159, https://doi.org/10.21236/ad1002455

Valladares, C. E., & Hei, M. A. (2012). Measurement of the characteristics of TIDs using small and regional networks of GPS receivers during the campaign of 17–30 July of 2008. *International Journal of Geophysics*, *2012*, A548784. https://doi.org/10.1155/2012/548784

Waliser, D. E., Graham, N. E., & Gautier, C. (1993). Comparison of the highly reflective cloud and outgoing longwave radiation datasets for use in estimating tropical deep convection. *Journal of Climate*, *6*(2), 331–353. https://doi.org/10.1175/1520-0442

Watthanasangmechai, K., Yamamoto, M., Saito, A., Tsunoda, R., Yokoyama, T., Supnithi, P., et al. (2016). Predawn plasma bubble cluster observed in Southeast Asia. *Journal of Geophysical Research: Space Physics*, *121*, 5868–5879. https://doi.org/10.1002/2015JA022069

Woodman, R. F., & LaHoz, C. (1976). Radar observations of *F* region equatorial irregularities. *Journal of Geophysical Research*, *81*(31), 5447–5466. https://doi.org/10.1029/JA081i031p05447

Xiao, Z., Xiao, S., Hao, Y., & Zhang, D. (2007). Morphological features of ionospheric response to typhoon. *Journal of Geophysical Research*, *112*, A04304. https://doi.org/10.1029/2006JA011671

Yang, Z., & Liu, Z. (2016). Observational study of ionospheric irregularities and GPS scintillations associated with the 2012 tropical cyclone Tembin passing Hong Kong. *Journal of Geophysical Research: Space Physics*, *121*, 4705–4717. https://doi.org/10.1002/2016JA022398

Yokoyama, T., Fukao, S., & Yamamoto, M. (2004). Relationship of the onset of equatorial *F* region irregularities with the sunset terminator observed with the Equatorial Atmosphere Radar. *Geophysical Research Letters*, *31*, L24804. https://doi.org/10.1029/2004GL021529

Yokoyama, T., Jin, H., Shinagawa, H., & Liu, H. (2019). Seeding of equatorial plasma bubbles by vertical neutral wind. *Geophysical Research Letters*, *46*, 7088–7095. https://doi.org/10.1029/2019GL083629